Chemical Engineering Journal 320 (2017) 124–134

Contents lists available at ScienceDirect

Chemical Engineering Journal

journal homepage: www.elsevier.com/locate/cej

Morphology-dependent properties of Co_3O_4/CeO_2 catalysts for low temperature dibromomethane (CH_2Br_2) oxidation

Jian Mei, Yu Ke, Zhongjue Yu, Xiaofang Hu, Zan Qu, Naiqiang Yan *

School of Environmental Science and Engineering, Shanghai Jiao Tong University, 800 Dong Chuan Road, Shanghai 200240, PR China

HIGHLIGHTS

- Co_3O_4/CeO_2-rod exhibited the high catalytic activity of CH_2Br_2 oxidation.
- CeO_2 morphology strongly affected Co_3O_4-CeO_2 interactions and structures of Co_3O_4/CeO_2 catalysts.
- Co^{3+} species, surface-adsorbed oxygen and oxygen vacancies were most abundant on Co_3O_4/CeO_2-rod.
- The reaction mechanism for CH_2Br_2 oxidation over Co_3O_4/CeO_2 catalysts was proposed.

GRAPHICAL ABSTRACT

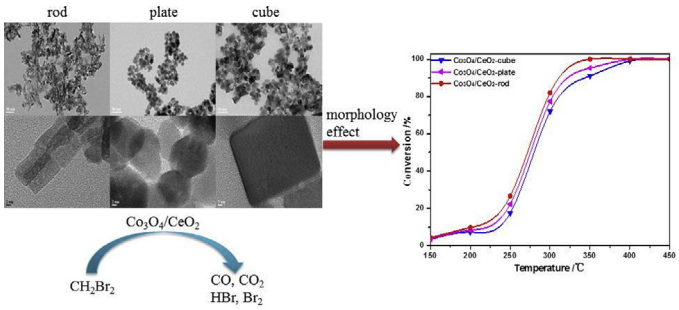

ARTICLE INFO

Article history:
Received 17 January 2017
Received in revised form 10 March 2017
Accepted 11 March 2017
Available online 14 March 2017

Keywords:
Dibromomethane
Co_3O_4
CeO_2 nanocrystals
Metal-support interaction

ABSTRACT

Brominated hydrocarbons are a typical pollutant in purified terephthalic acid (PTA) exhaust gas, which is harmful for human health and the environment once released to the atmosphere. In this study, three Co_3O_4/CeO_2 catalysts with different CeO_2 morphologies (rod, plate, and cube) were prepared and were used for low temperature dibromomethane (CH_2Br_2) oxidation, which was used as the model compound for brominated hydrocarbons. The experimental results showed that Co_3O_4/CeO_2-rod achieved significantly higher catalytic activity, with a T-90 of approximately 312 °C for CH_2Br_2 oxidation and higher selectivity to CO_2 than Co_3O_4/CeO_2-plate and Co_3O_4/CeO_2-cube. All of the Co_3O_4/CeO_2 catalysts investigated were stable for at least 30 h at 500 ppm CH_2Br_2 and 10% O_2 at a GHSV of 75,000 mL/(g·h)$^{-1}$, and the final products were CO_x, Br_2, and HBr, without the formation of other Br-containing organic byproducts. The higher catalytic activity of Co_3O_4/CeO_2-rod was attributed to the high content of Co^{3+}, more surface-adsorbed oxygen, and more oxygen vacancies in their exposed {100} and {110} planes. In addition, Co_3O_4 had a stronger interaction with CeO_2-rod, making it superior for CH_2Br_2 oxidation. Moreover, on the basis of the analysis of products and *in situ* DRIFTS studies, a credible reaction mechanism for CH_2Br_2 oxidation over Co_3O_4/CeO_2 catalysts was proposed.

1. Introduction

Volatile organic compounds (VOCs) not only are recognized as one of potent and important contributors to air pollution [1], but also put human health and the environment at risk [2]. Particularly, increasing attention is being paid to purified terephthalic acid (PTA) exhaust gas because of its high toxicity and difficulty of treatment [3], and the staging of massive protests against such projects in China in recent years. The PTA exhaust gas contains various organic compounds, such as p-xylene (PX), brominated hydrocarbons, and acetic acid methyl ester [4]. Among all of the treatment methods, catalytic oxidation is one of the most popular methods to treat PTA exhaust gas, by reason of its low energy

* Corresponding author.
E-mail address: nqyan@sjtu.edu.cn (N. Yan).

http://dx.doi.org/10.1016/j.cej.2017.03.038
1385-8947/

consumption and lower contents of secondary pollutants [5]. Nevertheless, the existence of brominated hydrocarbons in PTA exhaust gas demands that the catalyst must have the ability to resist bromine-poisoning. Therefore, the key issue in this method is to develop a high-performance catalyst to remove brominated hydrocarbons.

Currently, researchers are mainly focusing on two types of catalysts for brominated hydrocarbons oxidation, including noble metals [6] and transition metal oxides [3]. In spite of noble metal catalysts display prominent catalytic activity, the low resistance to bromine-poisoning and high cost limits their industrial applications. In contrast, transition metal oxide catalysts have gained increasing attention on account of their low cost, high catalytic activity, and high stability to brominated hydrocarbons oxidation. Thus, it is of great interest to develop transition metal oxide catalysts for brominated hydrocarbons oxidation.

Among many transition metal oxides, the Co-based catalyst has been proven to have a good catalytic performance for brominated hydrocarbons oxidation [7]. However, the catalytic activity, product-selectivity, and stability of the Co-based catalyst need to be further improved. CeO_2 is often used as a support in the catalytic reaction, such as CuO/CeO_2 [8], Au/CeO_2 [9], and $FeOOH/CeO_2$ [10], by reason of its prominent oxygen mobility [11], high oxygen storage capacity [12], and some acidic properties [13]. In addition, CeO_2 as a support can promote the dispersion of metal oxides and increase the metal-support interaction [14]. In the past few years, it has been found that the catalytic performance of CeO_2 is affected by exposed lattice planes [15]. Generally, different lattice planes are exposed in different CeO_2 morphologies. For instance, CeO_2 nanorods are prone to expose two {100} planes and four {110} planes [16], while CeO_2 nanocubes expose six {100} planes [17]. On the basis of density functional theory, the chemical activities of the different CeO_2 planes follow the order: {111} < {100} < {110}[18], which reveals that it is easier to produce oxygen vacancies on the CeO_2 {110} plane. Until now, there have been many reports about morphology effects of the CeO_2 support on dry-reforming of methane [18] and oxidation of CO [19]. It is reported that Co_3O_4/CeO_2 catalysts have been studied in the field of catalysis due to their unique physicochemical properties. For example, Guo et al. reported that Co_3O_4/meso-CeO_2 had a good catalytic performance for CO preferential oxidation in H_2-rich gases because of the high dispersion of cobalt oxides on meso-CeO_2 supports [20]. Tian et al. found that $(Co_3O_4)_{50\%}/CeO_2$ had a better reducibility and activity oxygen species, which coincided with its high catalytic activity for CO oxidation [21]. However, research about Co_3O_4/CeO_2 catalysts, relating the effect of CeO_2 morphology on the catalytic performance for brominated hydrocarbons oxidation, is rare.

In this study, Co_3O_4/CeO_2 catalysts with different CeO_2 morphologies (rod, plate, and cube) were prepared and were used for dibromomethane (CH_2Br_2) oxidation, which was chosen as the model compound for brominated hydrocarbons. The physicochemical properties of Co_3O_4/CeO_2 catalysts with different CeO_2 morphologies were studied. The CH_2Br_2 conversion, analysis of products, and catalyst stability were also investigated. On the basis of the analysis of products and *in situ* DRIFTS studies, a credible reaction mechanism for CH_2Br_2 oxidation over Co_3O_4/CeO_2 catalysts was proposed.

2. Experimental section

2.1. Catalyst preparation

CeO_2 nanorods and nanocubes were prepared by the hydrothermal method. Typically, 3.48 g $Ce(NO_3)_3{\cdot}6H_2O$ and 19.2 g NaOH were dissolved in 40 mL ultrapure water, respectively. Next, the NaOH solution was dripped into the $Ce(NO_3)_3$ solution, and the mixed solution was magnetic stirred for 60 min. Then, the mixed solution was transferred into a stainless steel reaction kettle with Teflon lining and maintained at constant temperatures (rods: 100 °C; and cubes: 180 °C) for 24 h.

CeO_2 nanoplates were prepared by the CTAB (Cetyltrimethyl Ammonium Bromide)-assisted hydrothermal method. Typically, 0.73 g CTAB and 2.61 g $Ce(NO_3)_3{\cdot}6H_2O$ were dissolved in 80 mL ultrapure water and magnetic stirred for 30 min. Subsequently, 8 mL $NH_3{\cdot}H_2O$ was dripped into the mixed solution and magnetic stirred for 30 min, and then the mixed solution was transferred into a stainless steel reaction kettle with Teflon lining and maintained at 100 °C for 24 h.

After filtering and washing with ultrapure water, the obtained precipitates were dried at 60 °C for 12 h, and then calcined at 500 °C for 3 h in air.

Co_3O_4/CeO_2 catalysts with different CeO_2 morphologies (rod, plate, and cube) were prepared by the impregnation method. CeO_2 powders were mixed with $Co(NO_3)_2{\cdot}6H_2O$ solution under magnetic stirring at 60 °C to gain Co_3O_4/CeO_2 (5 wt% Co/CeO_2). The samples were dried at 60 °C for 12 h, and then calcined at 500 °C for 3 h in air. The samples were flagged as CeO_2-rod, CeO_2-plate, CeO_2-cube, Co_3O_4/CeO_2-rod, Co_3O_4/CeO_2-plate, and Co_3O_4/CeO_2-cube.

2.2. Catalyst characterization

X-ray diffraction (XRD) were performed on the Shimadzu XRD-6100, and the diffractograms were obtained in the 2θ range of 10°–80°, with a scanning velocity of 10°/min. The N_2 adsorption-desorption isotherms were collected using a physical adsorption instrument (Nova 2200e) at −196 °C. Before each experiment, the samples were pretreated under the condition of vacuum at 200 °C for 3 h. The specific surface area was obtained by the multipoint BET model. Raman spectra were recorded on a SENTERRA R200 microscope. The excitation source was the 532 nm line of Ar ion laser. The morphology of the samples was observed using transmission electron microscopy (TEM) (JEOL-2100F) and scanning electron microscope (SEM) (JSM-7800F). Before each experiment, the samples were evenly dispersed in ethanol solution under the condition of ultrasound. Chemical analysis of the samples was performed on the inductively coupled plasma (ICP) spectrometer with iCAP 6000 Radial. The H_2-TPR experiments were performed on an automatic chemical adsorption instrument (AutoChem II, 2920). Before each experiment, the 100 mg samples were degassed in Ar flow at 300 °C for 2 h. Subsequently, after cooling to 100 °C, the samples were heated up to 1000 °C in 10% H_2/Ar flow, with a heating rate of 10 °C/min. The NH_3-TPD experiments were also performed on an automatic chemical adsorption instrument (AutoChem II, 2920). Before each experiment, the 500 mg samples were degassed in He flow at 300 °C for 2 h. Then, after cooling to 50 °C, NH_3 adsorption was performed in 10% NH_3/He flow at 50 °C for 1 h. Subsequently, the samples were treated in He flow for 30 min to remove gaseous NH_3, and then heated up to 800 °C in He flow, with a heating rate of 10 °C/min. X-ray photoelectron spectroscopy (XPS) was carried out on a PHI-5300 (PE) spectrometer using Mg Ka radiation as the excitation source, the binding energy was calibrated using the C 1 s line at 284.8 eV as an internal standard.

2.3. Catalytic performance evaluation

The catalytic performance for CH_2Br_2 oxidation was investigated by a fixed-bed flow reactor (i.d 6 mm). 120 mg catalyst was placed in the middle of the reactor using silica wool. The gas

mixture contained 500 ppm CH_2Br_2, 10% O_2, 0 or 2% H_2O, 0 or 500 ppm p-xylene (PX), and N_2 as the balance. The gaseous CH_2Br_2 was produced by a nitrogen-blowing method, passing N_2 flow through a bottle containing pure CH_2Br_2 in a thermostatic oil bath. The gaseous H_2O and PX were produced by the same method, respectively. The total gas flow was 150 mL/min, giving a gas hourly space velocity (GHSV) of 75,000 mL/(g·h)$^{-1}$. The range of catalytic temperatures was from 150 to 450 °C. The concentration of CH_2Br_2 was monitored by a GC-9790 equipped with a FID, and the data were collected at each evaluated temperature after stabilizing for 30 min. The catalytic activity was evaluated in terms of CH_2Br_2 conversion, defined as follows:

$$X_{CH_2Br_2} = \frac{C_{in} - C_{out}}{C_{in}} \times 100\% \quad (1)$$

where C_{in} and C_{out} are the CH_2Br_2 concentrations corresponding to the inlet and outlet, respectively.

The outlet gas products were determined by a GCMS-QP2010. The concentrations of Br_2 and HBr were determined by the titration method. The gas containing Br_2 and HBr was first absorbed in a KI solution of a certain concentration. Next, the concentration of Br_2 was determined by the titration using $Na_2S_2O_3$ solution with starch solution as an indicator. The concentration of bromide ions in the absorbed solution was determined by an ion chromatography. The concentrations of CO and CO_2 were monitored by a GC-14B equipped with a FID and a methane conversion oven. The selectivity to CO, CO_2, Br_2, and HBr were defined as follows, respectively:

$$S_{CO} = \frac{C_{co}}{C_{in} - C_{out}} \times 100\% \quad (2)$$

$$S_{CO_2} = \frac{C_{CO_2}}{C_{in} - C_{out}} \times 100\% \quad (3)$$

$$S_{Br_2} = \frac{C_{Br_2}}{C_{in} - C_{out}} \times 100\% \quad (4)$$

$$S_{HBr} = \frac{C_{HBr}}{2(C_{in} - C_{out})} \times 100\% \quad (5)$$

where C_{co} and C_{CO_2} are the concentrations of CO and CO_2 (ppm) in the outlet, C_{Br_2} and C_{HBr} are the concentrations of Br_2 and HBr (ppm) in the outlet.

2.4. In situ DRIFTS studies

In situ DRIFTS experiments were carried out on a Fourier transform infrared spectrometer (FTIR, Nicolet 6700) fitted with a MCT detector. The DRIFTS cell was fitted with ZnSe windows and a heating chamber. Real reaction conditions were simulated by a temperature controller and mass flow controllers. The *in situ* DRIFTS spectra were collected in the range of 4000–800 cm^{-1} at a resolution of 4 cm^{-1} and over 100 scans. Prior to each experiment, the samples were pretreated with 10% O_2/N_2 at 400 °C for 2 h to remove surface contaminants, and then cooled to 50 °C. Spectra of the clean catalyst surface were collected and used as the background. Next, a gas stream containing 500 ppm CH_2Br_2/10% O_2/N_2 was exposed to the DRIFTS cell at 50 °C for 1 h. Finally, the catalyst was treated in 10% O_2/N_2 from 50 to 400 °C. *In situ* DRIFTS spectra were collected from 50 to 400 °C.

3. Results and discussion

3.1. Catalytic performance

The activity of the CeO_2 and Co_3O_4/CeO_2 catalysts investigated for CH_2Br_2 oxidation is shown in Fig. 1. It is obvious that CH_2Br_2 conversion over all of the catalysts increased with the increase of temperature, and an apparent difference in the activity was also found. Pure CeO_2 supports exhibited considerable activity, particularly, the activity of CeO_2-rod was the highest among the three CeO_2 supports, with a T-90 (the temperature needed for 90% conversion) of approximately 370 °C, followed by CeO_2-plate and by CeO_2-cube, which was the least active. With the addition of Co, the activity was significantly improved and the conversion curves shifted to lower temperatures. Co_3O_4/CeO_2-rod exhibited the highest activity, with a T-90 of approximately 312 °C, followed by Co_3O_4/CeO_2-plate and by Co_3O_4/CeO_2-cube, which was the least active.

3.2. Catalyst characterization

Fig. 2 shows the TEM and HRTEM images of Co_3O_4/CeO_2 catalysts with different CeO_2 morphologies. The TEM images indicated that the three different CeO_2 catalysts still kept their original morphologies after the addition of Co. Fig. 2a displayed that Co_3O_4/CeO_2-rod was composed of nanorods with a width of approximately 10 nm and length varying from 20 to 100 nm. According to the HRTEM image (Fig. 2b), two types of lattice fringe directions, corresponded to (220) and (200) planes, were found for Co_3O_4/CeO_2-rod, which had interplanar spacing of 0.19 and 0.27 nm, respectively. Therefore, Co_3O_4/CeO_2-rod grew along the [110] direction and mainly exposed the unstable {110} and {100} planes [22]. The TEM image of Co_3O_4/CeO_2-plate displayed that it consisted of hexagonal plates with a diameter of approximately 18 nm (Fig. 2c). The HRTEM image in Fig. 2d displayed that the lattice fringe attributed to the (111) plane, with an interplanar spacing of 0.32 nm, belonged to the {111} plane [23]. The Co_3O_4/CeO_2-cube was cube with uneven size varying from 15 to 60 nm. The HRTEM image in Fig. 2f displayed that the lattice fringe assigned to the (200) plane with an interplanar spacing of 0.27 nm, belonged to the {100} plane. The morphology of Co_3O_4/CeO_2-cube matched with that of a cube exposed by six {100} planes [24]. Interestingly, the lattice fringes attributed to Co_3O_4 were not observed for all three Co_3O_4/CeO_2 catalysts, indicating

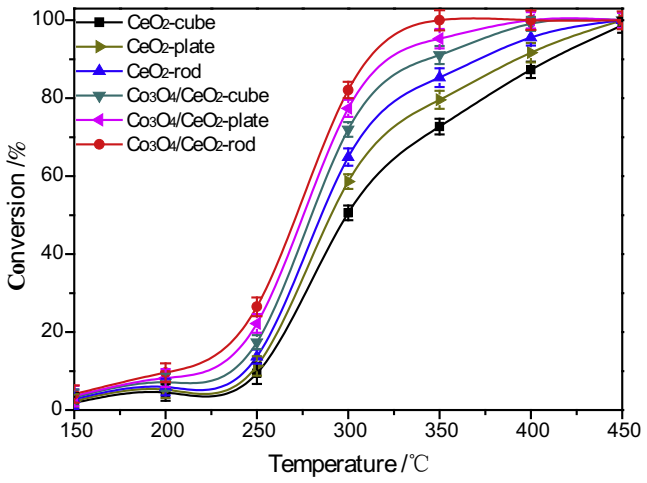

Fig. 1. Conversion curves for CH_2Br_2 oxidation as a function of temperature over the CeO_2 and Co_3O_4/CeO_2 catalysts investigated.

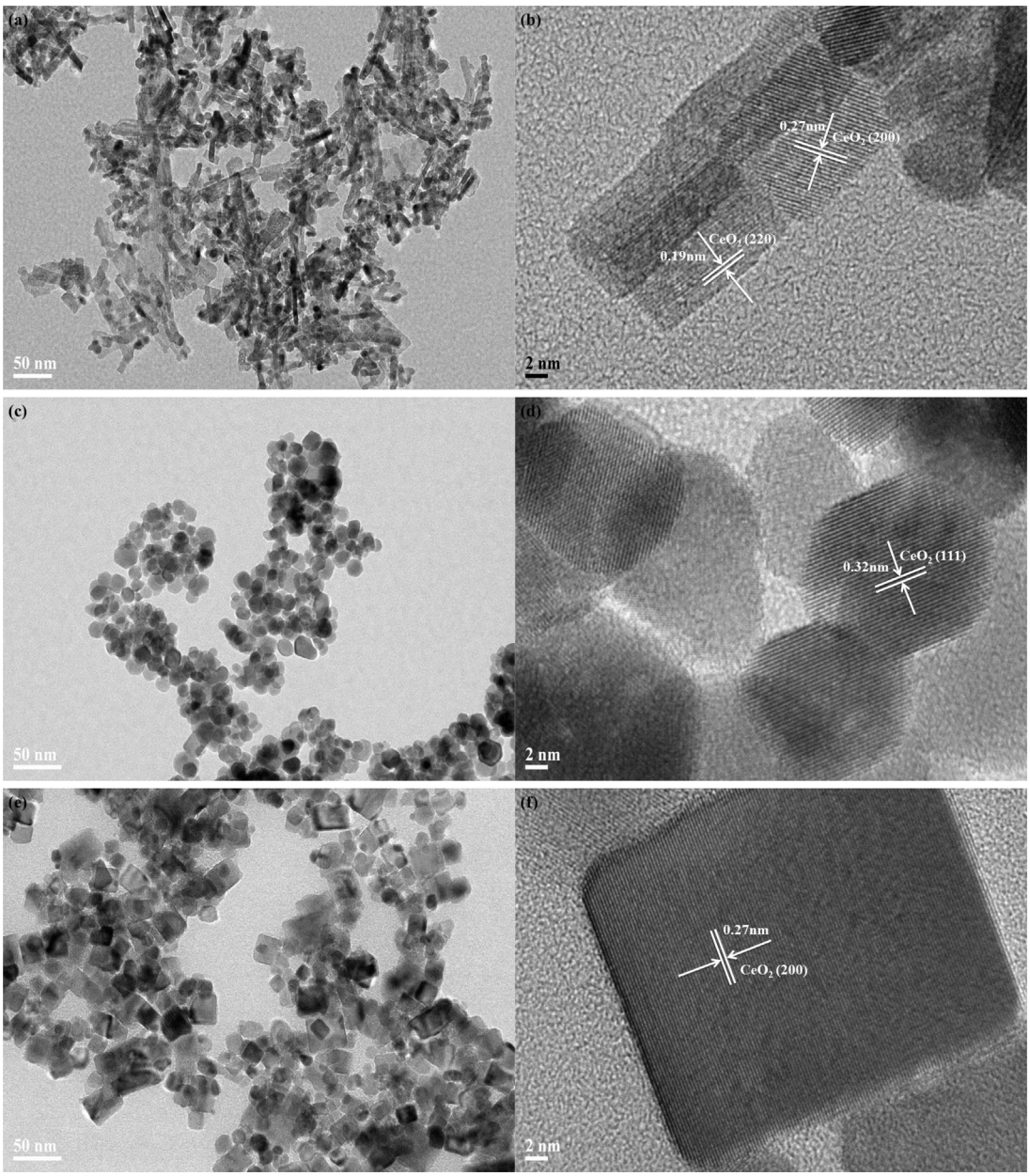

Fig. 2. TEM and HRTEM images of Co_3O_4/CeO_2-rod (a, b), Co_3O_4/CeO_2-plate (c, d), and Co_3O_4/CeO_2-cube (e, f).

that Co_3O_4 had a good dispersion on the surface of all three CeO_2 supports. To further obtain the morphology information of Co_3O_4/CeO_2 catalysts with different CeO_2 morphologies, SEM experiment was also conducted, and the images of SEM (Fig. S1) were consistent with those of TEM. The above results revealed that the desired morphologies of Co_3O_4/CeO_2 catalysts with different CeO_2 planes were successfully synthesized.

Fig. 3 shows the XRD patterns of the CeO_2 and Co_3O_4/CeO_2 catalysts investigated. The diffraction peaks at 28.5, 33.0, 47.5, 56.3, 59.1, 69.4, 76.8, and 79.1° were ascribed to the face-centered cubic fluorite structure of CeO_2 in all of the samples [25]. Interestingly, only a very weak peak at 36.9°, assigned to Co_3O_4 [26], was observed in Co_3O_4/CeO_2 catalysts, indicating thorough dispersion of Co_3O_4 or amorphous Co-containing species on the CeO_2 supports.

The chemical compositions of the CeO_2 and Co_3O_4/CeO_2 catalysts investigated were measured by ICP and the results were listed in Table 1. Co/CeO_2 mass ratios of the three Co_3O_4/CeO_2 catalysts were basically consistent with the nominal values. The N_2 adsorption-desorption isotherm and pore size distribution of the CeO_2 and Co_3O_4/CeO_2 catalysts investigated are shown in Fig. S2, and the physical properties estimated by N_2 physisorption were also listed in Table 1. As shown in Fig. S2(a), the N_2 adsorption-desorption isotherms of the CeO_2 and Co_3O_4/CeO_2 catalysts investigated were assigned to type IV with a type H3 hysteresis loop at high relative pressure. As shown in Fig. S2(b), it was found that the pore size distribution of the CeO_2 and Co_3O_4/CeO_2 catalysts investigated was not uniform and all the CeO_2 and Co_3O_4/CeO_2 catalysts investigated had porosity structures. As listed in Table 1, the average pore size of CeO_2-rod, CeO_2-plate, and CeO_2-cube were 25.1, 23.4, and 19.8 nm, respectively. With the addition of Co, the average pore size became small and decreased to 24.9, 22.2, and 18.3 nm for Co_3O_4/CeO_2-rod, Co_3O_4/CeO_2-plate, and Co_3O_4/CeO_2-cube, respectively. In addition, the pore size of Co_3O_4/CeO_2-rod,

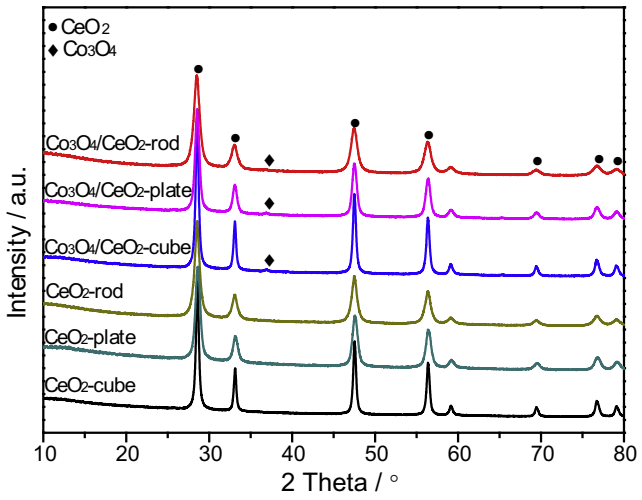

Fig. 3. XRD patterns of the CeO_2 and Co_3O_4/CeO_2 catalysts investigated.

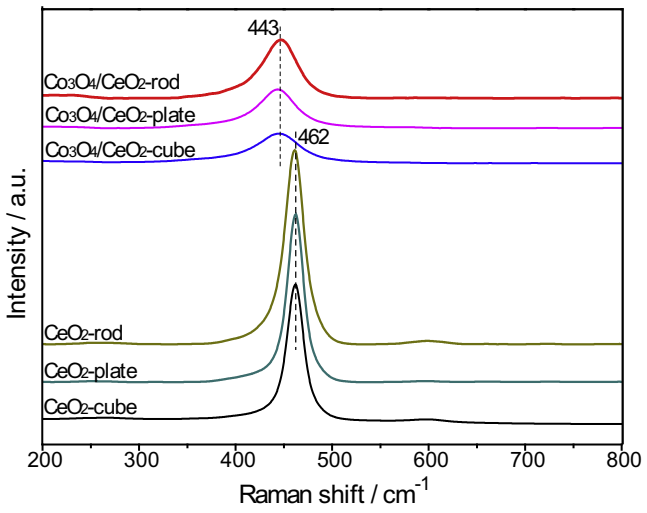

Fig. 4. Raman spectra of the CeO_2 and Co_3O_4/CeO_2 catalysts investigated.

Co_3O_4/CeO_2-plate, and Co_3O_4/CeO_2-cube was centered on approximately 3, 10, and 25 nm, respectively. Moreover, the specific surface area of CeO_2-rod, CeO_2-plate, and CeO_2-cube were 67.1, 52.9, and 26.8 $m^2\ g^{-1}$, respectively. After the addition of Co, the specific surface area of CeO_2-rod, CeO_2-plate, and CeO_2-cube decreased to 58.9, 44.7, and 15.4 $m^2\ g^{-1}$, respectively. The specific surface areas were consistent with the crystallite sizes calculated by the results of XRD where Co_3O_4/CeO_2-rod had the smallest Co_3O_4 particle size at approximately 10.44 nm while that for Co_3O_4/CeO_2-cube (approximately 16.50 nm) was the largest. The larger specific surface area of CeO_2-rod was beneficial for the dispersion of Co_3O_4, which was conducive to the catalytic performance.

Fig. 4 shows the Raman spectra of the CeO_2 and Co_3O_4/CeO_2 catalysts investigated. For pure CeO_2 supports, a distinct vibrational mode (F_{2g}) at 462 cm^{-1} was observed, which was belong to the symmetrical stretching vibration of the CeO_2 phase [27]. The maximum half width (MHW) values of the F_{2g} peaks were in the sequence of CeO_2-rod > CeO_2-plate > CeO_2-cube. Generally, the higher MHW values of the F_{2g} peaks, the higher concentrations of oxygen defects [18]. Thus, CeO_2-rod had the highest concentration of oxygen defects, followed by CeO_2-plate, and CeO_2-cube had the least. The Raman spectra of Co_3O_4/CeO_2 catalysts had similarities with those of CeO_2 catalysts. However, the bands assigned to cobalt oxide species were not found, which revealed that they were well dispersed. In addition, the presence of Co led to not only a slight red-shift of F_{2g} peaks from 462 to 443 cm^{-1} but also the increase of the MHW values. The red-shift together with band broadening revealed the incorporation of Co ions into the surface of CeO_2 supports, but without changing the original CeO_2 cubic structure, which resulted in the increase of oxygen vacancies.

Fig. 5 shows the H_2-TPR profiles of the CeO_2 and Co_3O_4/CeO_2 catalysts investigated. It can be seen that the CeO_2 supports only showed two reduction peaks, while Co_3O_4/CeO_2 catalysts showed three reduction peaks. For CeO_2 supports, the low-temperature reduction peak was assigned to the reduction of CeO_2 particles with small size while the high-temperature reduction peak was attributed to the reduction of particles with large size [28]. For Co_3O_4/CeO_2-rod, the former two reduction peaks at approximately 275 and 329 °C were assigned to the reduction of Co^{3+} to Co^{2+} and Co^{2+} to Co^0, respectively [29], while the last reduction peak was assigned to the reduction of CeO_2. Similar profiles were also observed for Co_3O_4/CeO_2-plate and Co_3O_4/CeO_2-cube, except that the reduction peaks shifted to higher temperatures. The results suggested that the interaction between Co_3O_4 and CeO_2-rod was the strongest among the three Co_3O_4/CeO_2 catalysts. As well known, the stronger the interaction between Co_3O_4 and CeO_2 supports, the higher the redox ability of cobalt species [30].

Fig. 6 shows the XPS spectra of Co 2p, Ce 3d, and O 1s for the Co_3O_4/CeO_2 catalysts investigated. As can be seen in Fig. 6(a), for the three Co_3O_4/CeO_2 catalysts, two main peaks ascribed to Co $2p_{3/2}$ and Co $2p_{1/2}$ at 781.5–782.7 and 797.0–798.1 eV, respectively, with satellite peaks, were observed. The Co $2p_{3/2}$ spectra could be decomposed into two characteristic peaks, of which the peak with the lower binding energy was corresponded to Co^{3+}, while the peak with the high binding energy was related to Co^{2+} [31]. According to Table 2, the proportion of Co^{3+} to the total Co

Table 1
The structural and physical properties of the CeO_2 and Co_3O_4/CeO_2 catalysts investigated.

Catalyst	Co/CeO_2 (wt%)	S_{BET} ($m^2\ g^{-1}$)	Da (nm)	V ($cm^3\ g^{-1}$)	$DCeO_2$ (nm)	DCo_3O_4 (nm)
Co_3O_4/CeO_2-rod	4.68	58.9	24.9	0.363	11.68	10.44
Co_3O_4/CeO_2-plate	4.71	44.7	22.2	0.264	14.63	13.21
Co_3O_4/CeO_2-cube	4.70	15.4	18.3	0.135	19.67	16.50
CeO_2-rod	–	67.1	25.1	0.461	13.38	–
CeO_2-plate	–	52.9	23.4	0.332	15.41	–
CeO_2-cube	–	26.8	19.8	0.244	20.52	–

Co/CeO_2: Co/CeO_2 mass ratio measured by ICP.
S_{BET}: Specific surface area estimated by N_2 physisorption.
Da: Average pore diameter estimated by N_2 physisorption.
V: Pore volume estimated by N_2 physisorption.
$DCeO_2$: CeO_2 crystallite size calculated by Scherrer equation from XRD.
DCo_3O_4: Co_3O_4 crystallite size calculated by Scherrer equation from XRD.

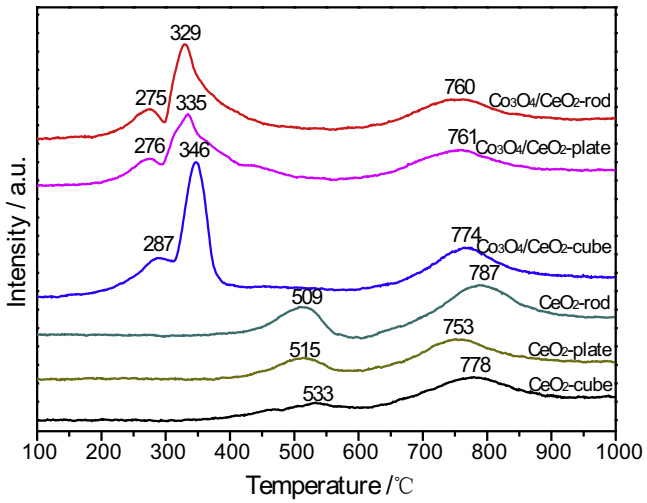

Fig. 5. H_2-TPR profiles of the CeO_2 and Co_3O_4/CeO_2 catalysts investigated.

on Co_3O_4/CeO_2-rod, Co_3O_4/CeO_2-plate, and Co_3O_4/CeO_2-cube was 0.66, 0.63, and 0.59, respectively. Thus, the proportion of Co^{3+} on Co_3O_4/CeO_2-rod was higher than that on Co_3O_4/CeO_2-plate and Co_3O_4/CeO_2-cube, and it is believed that the better catalytic performance of Co_3O_4/CeO_2-rod is associated with the high content of Co^{3+} [7].

Fig. 6(b) shows the XPS spectra of Ce 3d for the Co_3O_4/CeO_2 catalysts investigated. The spectra of Ce 3d could be resolved into eight peaks, of which six peaks denoted as v, v_2, v_3, u, u_2, and u_3 were assigned to Ce^{4+}, while the other two peaks, denoted as v_1 and u_1, were assigned to Ce^{3+} [32]. According to Table 2, the proportion of Ce^{3+} to the total Ce on Co_3O_4/CeO_2-rod, Co_3O_4/CeO_2-plate, and Co_3O_4/CeO_2-cube was 0.18, 0.15, and 0.11, respectively. It is reported that the transformation between Ce^{3+} and Ce^{4+} could produce oxygen vacancies in previous literatures, revealing that the higher the proportion of Ce^{3+}, the more oxygen vacancies are formed [33]. Combined with the results of Raman spectroscopy, the oxygen vacancies of Co_3O_4/CeO_2-rod were more than those of Co_3O_4/CeO_2-plate and Co_3O_4/CeO_2-cube. Therefore, it was likely that the better catalytic performance of Co_3O_4/CeO_2-rod was related to the higher proportion of Ce^{3+}.

The O 1s XPS spectra of Co_3O_4/CeO_2-rod, Co_3O_4/CeO_2-plate, and Co_3O_4/CeO_2-cube are shown in Fig. 6(c). The asymmetrical O 1s peak was divided into two components: one at BE = 528.8–529.1 eV was corresponded to the surface-lattice oxygen (O_{lat}), and the other at BE = 531.2–531.6 eV was related to the surface-adsorbed oxygen (O_{ads}) [7,34]. According to Table 2, the ratio of $O_{ads}/(O_{ads} + O_{lat})$ for Co_3O_4/CeO_2-rod was higher than those for Co_3O_4/CeO_2-plate and Co_3O_4/CeO_2-cube, revealing Co_3O_4/CeO_2-rod had more surface adsorbed oxygen, which was beneficial for catalytic oxidation.

3.3. Analysis of products

It is learned that the desired decomposition products of brominated hydrocarbons are CO_2 and Br_2 or HBr. To our disappointments, almost none of the treatment technologies can achieve complete mineralization. In this study, the products after reaction at different temperature over Co_3O_4/CeO_2-rod, Co_3O_4/CeO_2-plate, and Co_3O_4/CeO_2-cube were determined by GCMS, which are shown in Tables 3, S1, and S2. As can be seen in Table 3, for Co_3O_4/CeO_2-rod, the products were CO, CO_2, HBr, and H_2O at low temperatures (below 200 °C), while Br_2 was generated above 250 °C. Of particular note is that no other bromine products were generated at each

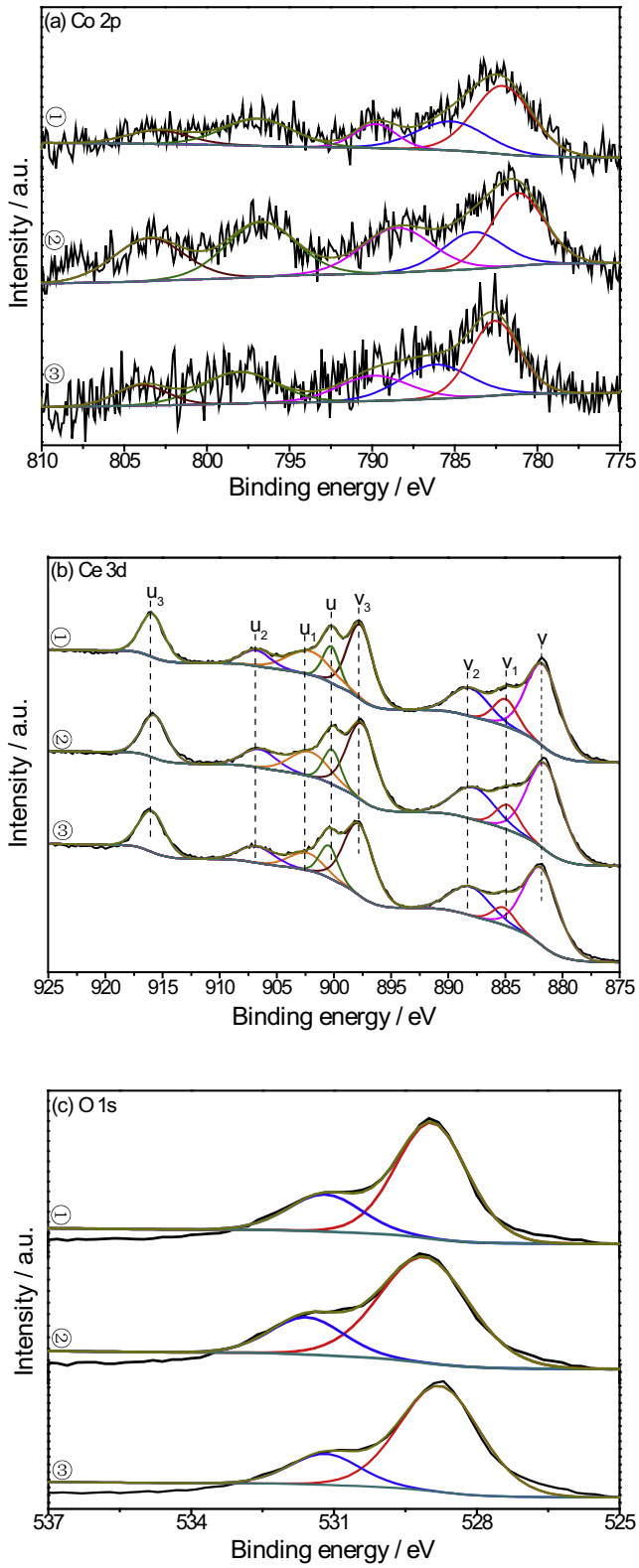

Fig. 6. XPS spectra of (a) Co 2p, (b) Ce 3d and (c) O 1 s for Co_3O_4/CeO_2 catalysts: ① Co_3O_4/CeO_2-rod, ② Co_3O_4/CeO_2-plate and ③ Co_3O_4/CeO_2-cube.

evaluated temperature. Moreover, exactly the same results were also observed for Co_3O_4/CeO_2-plate and Co_3O_4/CeO_2-cube, as shown in Tables S1 and S2, respectively.

It is also necessary to investigate the selectivity to CO, CO_2, HBr, and Br_2. Fig. 7 shows the selectivity to CO, CO_2, Br_2, and HBr as a

Table 2
XPS parameters of the Co_3O_4/CeO_2 catalysts investigated.

Catalyst	Surface composition (at.%)			$Co^{3+}/(Co^{2+} + Co^{3+})$	$Ce^{3+}/(Ce^{3+} + Ce^{4+})$	$O_{ads}/(O_{ads} + O_{lat})$	Co/Ce
	Co	Ce	O				
Co_3O_4/CeO_2-rod	0.71	6.89	53.54	0.66	0.18	0.25	0.13
Co_3O_4/CeO_2-plate	0.87	6.19	54.33	0.63	0.15	0.22	0.14
Co_3O_4/CeO_2-cube	0.98	8.92	51.71	0.59	0.11	0.20	0.11

Table 3
Products in outlet at different temperature over Co_3O_4/CeO_2-rod.

Temperature (°C)	Detected substances
150	CH_2Br_2, CO, CO_2, HBr, H_2O
200	CH_2Br_2, CO, CO_2, HBr, H_2O
250	CH_2Br_2, CO, CO_2, HBr, Br_2, H_2O
300	CH_2Br_2, CO, CO_2, HBr, Br_2, H_2O
350	CO, CO_2, HBr, Br_2, H_2O
400	CO, CO_2, HBr, Br_2, H_2O
450	CO, CO_2, HBr, Br_2, H_2O

function of temperature over the Co_3O_4/CeO_2 catalysts investigated. It was found that their selectivity were different, depending on the catalysts used. As can be seen in Fig. 7(a), for Co_3O_4/CeO_2-cube, when the temperature increased, the selectivity to CO and HBr gradually decreased, while that to CO_2 and Br_2 gradually increased. Similar results were also observed for Co_3O_4/CeO_2-plate and Co_3O_4/CeO_2-rod. The increase of CO_2 was due to further oxidation of CO, and the generation of Br_2 might be assigned to the Deacon reaction ($4HBr + O_2 = 2Br_2 + 2H_2O$) [7]. For Co_3O_4/CeO_2-cube, the selectivity to CO_2 and Br_2 were approximately 76% and 54%, respectively, at 350 °C, while the selectivity to CO_2 and Br_2 were approximately 80% and 65%, respectively, at 350 °C for Co_3O_4/CeO_2-plate, and approximately 84% and 69%, respectively, at 350 °C for Co_3O_4/CeO_2-rod. The results revealed that Co_3O_4/CeO_2-rod had the highest selectivity to CO_2 and Br_2 among the three Co_3O_4/CeO_2 catalysts.

3.4. The effect of water or p-xylene (PX)

Water vapor usually exists in the PTA exhaust gas, and it is necessary to consider the resistance of the catalyst to humidity. Thus, the CH_2Br_2 oxidation was performed in the presence of 2 vol% H_2O. As shown in Fig. 8 at low temperatures, the CH_2Br_2 conversion slightly increased when H_2O was present, and T-10 (the temperature needed for 10% conversion) decreased by approximately 10 °C. It was most likely that the promotional effect of H_2O on CH_2Br_2 oxidation at low temperatures was on account of the removal of surface bromine species, based on the reverse Deacon reaction: $H_2O + Br^- \leftrightharpoons HBr\uparrow + OH^-$ [3]. However, a decrease in CH_2Br_2 conversion was observed at high temperatures, due to the occupation of H_2O on a part of active sites.

Commonly, there are many organic compounds in PTA exhaust gas. However, it is not realistic to simultaneously study the effect of all of the organic compounds on CH_2Br_2 oxidation. Hence, we mainly focused on the characteristics of reactions involving binary organic pollutants. Thus, the effect of p-xylene (PX) on CH_2Br_2 oxidation over Co_3O_4/CeO_2-rod was also investigated. As shown in Fig. 8, the CH_2Br_2 conversion was obviously inhibited when PX was present, both at low and high temperatures, and T-90 shifted to 355 °C, which might be due to the decrease of oxygen species caused by consumption of surface-active oxygen during PX oxidation.

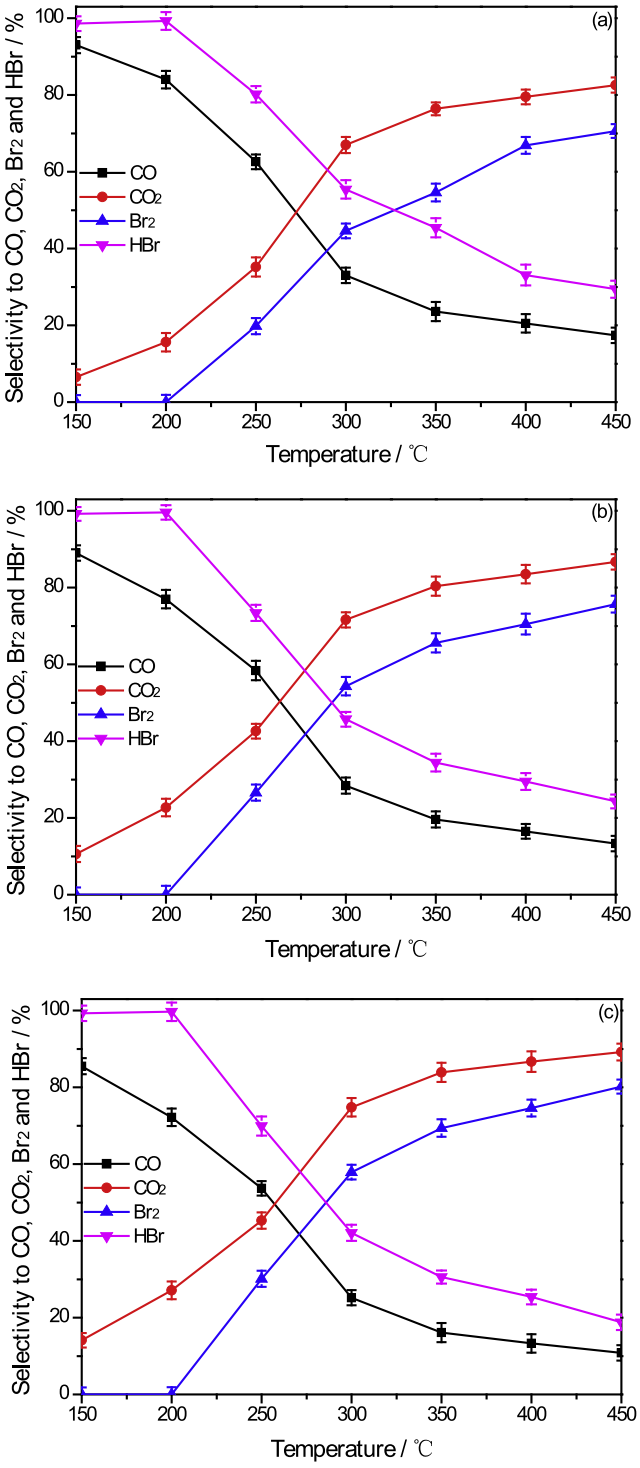

Fig. 7. Selectivity to CO, CO_2, Br_2, and HBr as a function of temperature over Co_3O_4/CeO_2-cube (a), Co_3O_4/CeO_2-plate (b), and Co_3O_4/CeO_2-rod (c).

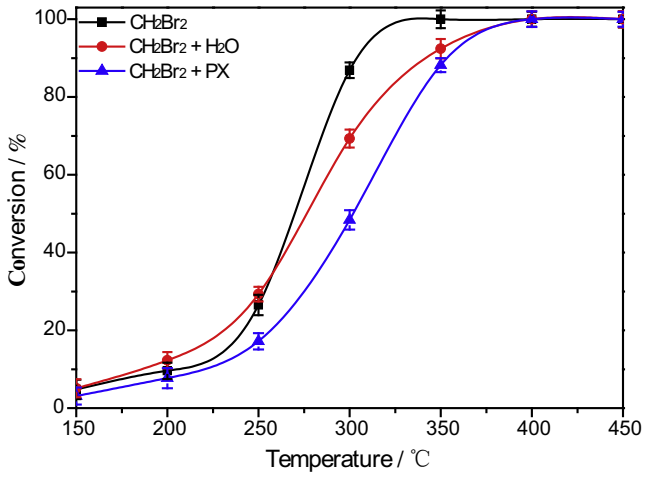

Fig. 8. The effect of water or p-xylene (PX) on CH_2Br_2 oxidation over Co_3O_4/CeO_2-rod; CH_2Br_2 alone: 500 ppm CH_2Br_2; $CH_2Br_2 + H_2O$: 500 ppm CH_2Br_2 + 2 vol% H_2O; CH_2Br_2 + PX: 500 ppm CH_2Br_2 + 500 ppm PX; in all cases, 10% O_2 and N_2 balance; GHSV = 75,000 mL/(g·h)$^{-1}$.

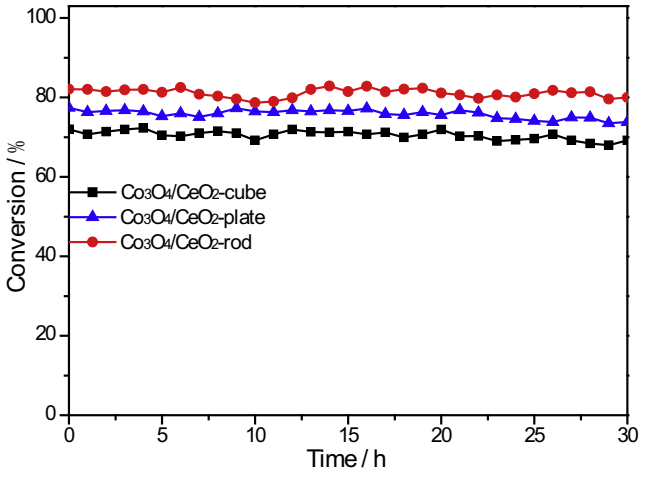

Fig. 9. Stability test of the Co_3O_4/CeO_2 catalysts with different morphologies at 300 °C.

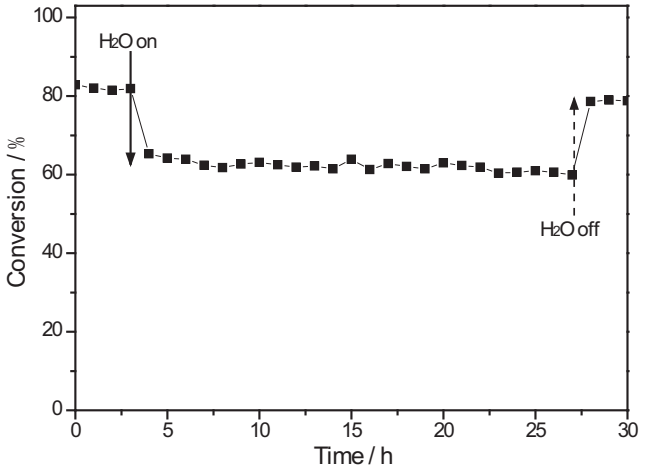

Fig. 10. Stability test of Co_3O_4/CeO_2-rod in the presence of 2 vol% water at 300 °C.

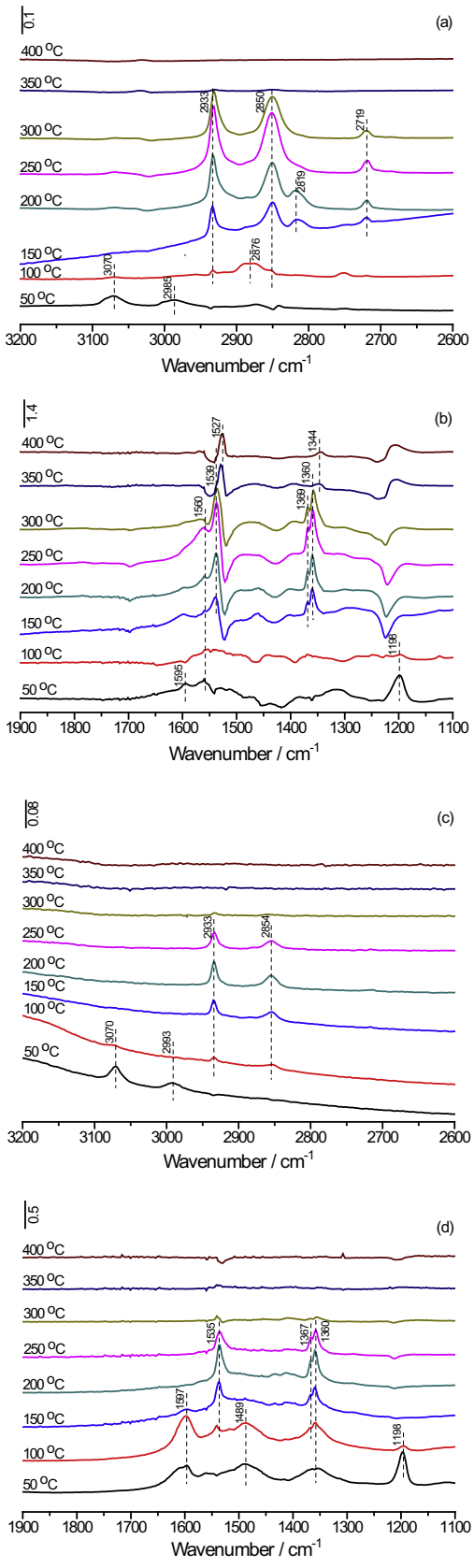

Fig. 11. *In situ* DRIFTS spectra of CH_2Br_2 oxidation over CeO_2-rod (a, b) and Co_3O_4/CeO_2-rod (c, d) catalysts at different temperatures.

3.5. Catalyst stability

To examine the catalytic stability, a long-duration CH_2Br_2 oxidation test was performed at a constant temperature. The on-stream evolution of CH_2Br_2 conversion with time at 300 °C for Co_3O_4/CeO_2 catalysts with different CeO_2 morphologies is shown in Fig. 9. Within 30 h, Co_3O_4/CeO_2-rod presented a stable conversion of approximately 82%. During the long-duration CH_2Br_2 oxidation test, the selectivity of product was nearly constant, revealing that the composition and structure of the active component was stable. In addition, there is a popular belief that the catalytic activity of Co-based catalyst is reduced due to the accumulation of Br species. XPS analysis (Fig. S4) indicated the deposition of only 1.2% Br on the surface of Co_3O_4/CeO_2-rod after 30 h of reaction, which might be ascribed to the fast reaction of Br species on the surface of Co_3O_4/CeO_2-rod. Moreover, Co_3O_4/CeO_2-plate and Co_3O_4/CeO_2-cube also showed good catalytic stability. The results revealed that all of the three Co_3O_4/CeO_2 catalysts were stable for CH_2Br_2 oxidation.

The stability of Co_3O_4/CeO_2-rod in the presence of 2 vol% water at 300 °C was also investigated. As shown in Fig. 10, the CH_2Br_2 conversion was always stabilized at approximately 82% within the first 3 h. Then, after the introduction of H_2O (2 vol%), an apparent decrease in CH_2Br_2 conversion from 82% to 62% occurred, revealing that H_2O showed a suppression effect on the catalytic reaction, on account of the competitive adsorption of CH_2Br_2 and H_2O on the active sites. The catalytic activity of Co_3O_4/CeO_2-rod was stabilized within 24 h. When H_2O was cut off, the CH_2Br_2 conversion basically regained its value of 82%. The results revealed that the catalytic activity of Co_3O_4/CeO_2-rod was sustainable and showed good resistance to water-penetration.

3.6. In situ DRIFTS studies

To get a deep insight into the catalytic behaviors of CeO_2 and Co_3O_4/CeO_2 catalysts, *in situ* DRIFTS experiments were carried out, and the results are displayed in Fig. 11. As can be seen in Fig. 11(a, b), for CeO_2-rod, after treated in the mixture of 500 ppm CH_2Br_2, 10% O_2, and N_2 at 50 °C for 1 h, the DRIFTS spectra exhibited bands at 3070, 2985, 1595, 1560, and 1198 cm^{-1}. The bands at 3070, 2985, and 1198 cm^{-1} were assigned to antisymmetric stretching, symmetric stretching, and wagging of methylene species (–CH_2–), respectively, in CH_2Br_2 molecules [35]. When the temperature increased, these bands gradually decreased in intensities and could not be observed above 100 °C, revealing either desorption or reaction of CH_2Br_2 molecules. The band at 1560 cm^{-1} was ascribed to the formate species (–COOH) [7]. The band at 1595 cm^{-1} was attributed to H_2O on the surface of CeO_2 [36], which was gradually removed when the temperature increased. In addition, the removal of the bands assigned to CH_2Br_2 molecules was along with the appearance of some new bands at 2933, 2876, 2850, 2819, 2719, 1539, 1369, and 1360 cm^{-1}. The bands at 2876, 2850, 2719, 1539, 1369, and 1360 cm^{-1} (including 1527 and 1344 cm^{-1} developed at 350 and 400 °C) were assigned to the formate species (–COOH) [3,37,38], while the other bands at 2933 and 2819 cm^{-1} were related to methyl antisymmetric stretching and symmetric stretching of the methoxy species (–CH_3O), respectively [39]. All of the bands generated with the decomposition of the absorbed CH_2Br_2, revealing that the formate and methoxy species were the main intermediate products produced on the surface of CeO_2-rod.

On the basic of *in situ* DRIFTS experiments, a believable reaction pathway for CH_2Br_2 oxidation over CeO_2 is shown in Fig. S5. The reaction pathway is described as follows: (1) A CH_2Br_2 molecule is adsorbed on oxygen vacancies through two bromine atoms. (2) The two bromine atoms are extracted by the adjacent nucleophilic oxygen, forming bidentate methoxy species, which were not observed due to their instability. (3) Formate and methoxy species are formed by the Cannizzaro type disproportionation of bidentate methoxy species. (4) The formate and methoxy species are further oxidized by active oxygen species to produce CO and CO_2.

In the case of Co_3O_4/CeO_2-rod (Fig. 11(c, d)), the similar DRIFTS spectra were observed at 50, 100, 150, 200, and 250 °C, except that some bands assigned to the formate species disappeared and a new band was observed at 1489 cm^{-1}, assigned to scissoring of methylene species (–CH_2–) [39], which revealed that the reaction pathway was not fundamentally changed by the addition of Co. When the temperature increased, the band intensity was decreased obviously at 250 °C and complete disappeared at 300 °C. The results revealed that the presence of Co further promoted the decomposition of intermediate species at high temperatures. Furthermore, no bands corresponding to CO, CO_2, and HBr as the final products could be observed, due to the quick desorption of these species.

For Co_3O_4/CeO_2 catalysts, the dissociation of C-Br and C–H bonds was easier on account of the electrophilicity and high valence of Co_3O_4, and the high catalytic activity was ascribed to the strong interaction between Co_3O_4 and CeO_2. In the process of reaction, Co^{3+} was reduced to Co^{2+}, after which the lattice oxygen of CeO_2 transferred to Co to reoxidize Co^{2+} to Co^{3+}. At the same time, CeO_2 released lattice oxygen that could be quickly reoxidized by gas-phase oxygen due to its excellent oxygen storage capacity. To get a deeper understanding of the reaction, a credible reaction mechanism for CH_2Br_2 oxidation over Co_3O_4/CeO_2 catalysts, consisting of five steps, is schematized in Fig. 12: (1) A CH_2Br_2 molecule is adsorbed on oxygen vacancies through two bromine atoms. (2) The two bromine atoms are extracted by the adjacent nucleophilic oxygen, forming bidentate methoxy species, which were not observed due to their instability. (3) The gas-phase oxygen is adsorbed on the catalyst surface to supplement the con-

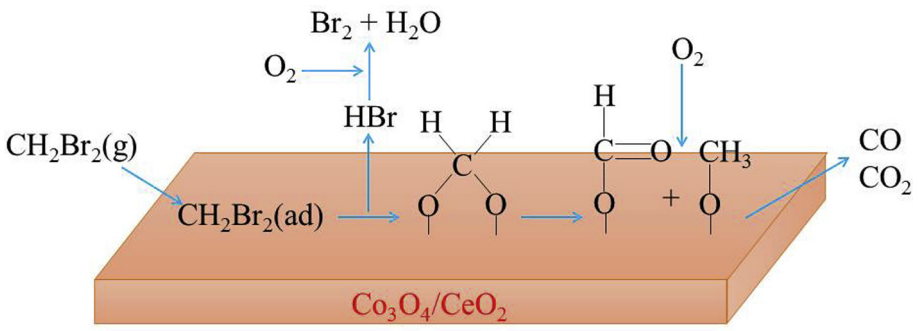

Fig. 12. A credible reaction mechanism for CH_2Br_2 oxidation over Co_3O_4/CeO_2 catalysts.

sumed oxygen. (4) Formate and methoxy species are formed by the Cannizzaro type disproportionation of bidentate methoxy species. (5) Formate and methoxy species are further oxidized by active oxygen species to generate CO and CO_2. Additionally, the Br species are quickly removed from the Co_3O_4/CeO_2 surface in the form of Br_2 by the Deacon reaction ($4HBr + O_2 = 2Br + HBr$), or in the form of HBr by the chemical reaction of the dissociatively adsorbed Br and surface hydroxyl groups.

4. Conclusions

Three Co_3O_4/CeO_2 catalysts with different CeO_2 morphologies (rod, plate, and cube) were prepared by the hydrothermal and impregnation methods, and the morphology effect of CeO_2 on the catalytic performance of Co_3O_4/CeO_2 catalysts for CH_2Br_2 oxidation, used as the model compound for brominated hydrocarbons, was investigated. Among the three Co_3O_4/CeO_2 catalysts, Co_3O_4/CeO_2-rod achieved significantly higher catalytic activity, with a T-90 of approximately 312 °C for CH_2Br_2 oxidation and higher selectivity to CO_2 than Co_3O_4/CeO_2-plate and Co_3O_4/CeO_2-cube. The HRTEM images revealed that the Co_3O_4/CeO_2-rod predominately exposed {1 0 0} and {1 1 0} planes. Based on the results of Raman and XPS, the Co, Ce valences, surface oxygen species, and oxygen vacancies were dependent on morphology. The high catalytic activity of Co_3O_4/CeO_2-rod was attributed to the high content of Co^{3+}, more surface-adsorbed oxygen, and more oxygen vacancies related to their exposed {1 0 0} and {1 1 0} planes. In addition, Co_3O_4 had a strong interaction with CeO_2-rod, making it superior for CH_2Br_2 oxidation. The results of long-duration stability experiments confirmed that Co_3O_4/CeO_2-rod could be considered as an excellent catalyst for CH_2Br_2 oxidation. Moreover, on the basis of the analysis of products and *in situ* DRIFTS studies, a credible reaction mechanism for CH_2Br_2 oxidation over Co_3O_4/CeO_2 catalysts was proposed.

Acknowledgements

This work was supported by the Major State Basic Research Development Program of China (973 Program, No. 2013CB430005), the National Natural Science Foundation of China (No. 51278294 and 21607102), and China's Post-doctoral Science Fun (No. 2015M581626).

Appendix A. Supplementary data

Supplementary data associated with this article can be found, in the online version, at http://dx.doi.org/10.1016/j.cej.2017.03.038.

References

[1] L. Ren, Y. Li, J. Hou, J. Bai, M. Mao, M. Zeng, X. Zhao, N. Li, The pivotal effect of the interaction between reactant and anatase TiO2 nanosheets with exposed 001 facets on photocatalysis for the photocatalytic purification of VOCs, Appl. Catal. B 181 (2016) 625–634.
[2] A. Tang, L. Hu, X. Yang, Y. Jia, Y. Zhang, Promoting effect of the addition of Ce and Fe on manganese oxide catalyst for 1, 2-dichlorobenzene catalytic combustion, Catal. Commun. 82 (2016) 41–45.
[3] J. Mei, S. Zhao, W. Huang, Z. Qu, N. Yan, Mn-Promoted Co_3O_4/TiO_2 as an efficient catalyst for catalytic oxidation of dibromomethane CH_2Br_2, J. Hazard. Mater. 318 (2016) 1–8.
[4] M. Moreton, Catalytic oxidation for PTA plant emissions control, Int. J. Hydrocarbon Eng. 3 (1998) 57–58.
[5] X.-X. Hao, H.-Z. Wang, X.-N. Wang, X. Wang, Z.-S. Liu, Overview of PTA off-gas treatment techniques, Contemp. Chem. Ind. 2 (2013) 020.
[6] X. Liu, J. Zeng, J. Wang, W. Shi, T. Zhu, Catalytic oxidation of methyl bromide using ruthenium-based catalysts, Catal. Sci. Technol. 6 (2016) 4337–4344.
[7] J. Mei, S. Zhao, H. Xu, Z. Qu, N. Yan, The performance and mechanism for the catalytic oxidation of dibromomethane (CH_2Br_2) over Co_3O_4/TiO_2 catalysts, RSC Adv. 6 (2016) 31181–31190.
[8] P.S. Barbato, S. Colussi, A. Di Benedetto, G. Landi, L. Lisi, J. Llorca, A. Trovarelli, On the origin of high activity and selectivity of CuO/CeO_2 catalysts prepared by solution combustion synthesis in CO-PROX reaction, J. Phys. Chem. C 120 (2016) 13039–13048.
[9] A.M. Abdel-Mageed, G. Kučerová, A.A. El-Moemen, J. Bansmann, D. Widmann, R.J. Behm, Geometric and electronic structure of Au on Au/CeO_2 catalysts during the CO oxidation: deactivation by reaction induced particle growth, J. Phys: Conf. Ser. 712 (2016) 012044.
[10] J.X. Feng, S.H. Ye, H. Xu, Y.X. Tong, G.R. Li, Design and synthesis of $FeOOH/CeO_2$ heterolayered nanotube electrocatalysts for the oxygen evolution reaction, Adv. Mater. 28 (2016) 4698–4703.
[11] P. Sudarsanam, B. Hillary, B. Mallesham, B.G. Rao, M.H. Amin, A. Nafady, A.M. Alsalme, B.M. Reddy, S.K. Bhargava, Designing CuOx nanoparticle-decorated CeO_2 nanocubes for catalytic soot oxidation: role of the nanointerface in the catalytic performance of heterostructured nanomaterials, Langmuir 32 (2016) 2208–2215.
[12] F. Wang, S. He, H. Chen, B. Wang, L. Zheng, M. Wei, D.G. Evans, X. Duan, Active site-dependent reaction mechanism over Ru/CeO_2 catalyst toward CO_2 methanation, J. Am. Chem. Soc. 138 (2016) 6298–6305.
[13] B.C. Shin, Ho Hwan, Jin-Sun Cha, Min-Chul Shin, Heesoo Lee, Physico-chemical property and catalytic activity of a CeO_2-Doped MnOx-TiO_2 Catalyst with SO_2 resistance for low-temperature NH_3-SCR of NOx, J. Nanosci. Nanotechnol. 16 (2016) 4370–4376.
[14] A. Ramli, M.F. Mohamad, S. Yusup, T.Y.Y. Hin, Hydrogen production from gasification of palm kernel shell in the presence of Fe/CeO_2 catalysts, Malaysian J. Anal. Sci. 20 (2016) 303–308.
[15] W. Huang, Y. Gao, Morphology-dependent surface chemistry and catalysis of CeO_2 nanocrystals, Catal. Sci. Technol. 4 (2014) 3772–3784.
[16] X. Du, D. Zhang, L. Shi, R. Gao, J. Zhang, Morphology dependence of catalytic properties of Ni/CeO_2 nanostructures for carbon dioxide reforming of methane, J. Phys. Chem. C 116 (2012) 10009–10016.
[17] Z. Liu, S. Guo, C. Hong, Z. Xia, Synthesis and photocatalytic properties of CeO_2 nanocubes, J. Mater. Sci.: Mater. Electron. 27 (2016) 2146–2150.
[18] N. Wang, W. Qian, W. Chu, F. Wei, Crystal-plane effect of nanoscale CeO_2 on the catalytic performance of Ni/CeO_2 catalysts for methane dry reforming, Catal. Sci. Technol. 6 (2016) 3594–3605.
[19] X. Guo, R. Zhou, A new insight into the morphology effect of ceria on CuO/CeO_2 catalysts for CO selective oxidation in hydrogen-rich gas, Catal. Sci. Technol. 6 (2016) 3862–3871.
[20] Q. Guo, W.U. Meiling, Y. Liu, X. Bai, Mesoporous CeO_2-supported Co_3O_4 catalysts for CO preferential oxidation in H_2 rich gases, Chin. J. Catal. 28 (2007) 953–957.
[21] J.J. Tian, W. Na, H. Wang, W.G. Gao, Low temperature CO oxidation over cobalt catalysts supported on mesoporous CeO_2, Adv. Mater. Res. 643 (2013) 76–82.
[22] S.A. Mock, S.E. Sharp, T.R. Stoner, M.J. Radetic, E.T. Zell, R. Wang, CeO_2 nanorods-supported transition metal catalysts for CO oxidation, J. Colloid Interface Sci. 466 (2016) 261–267.
[23] S. Darbha, Direct synthesis of dimethyl carbonate from CO_2 and methanol over CeO_2 catalysts of different morphologies, J. Chem. Sci. 128 (2016) 957–965.
[24] S. Fernandez-Garcia, L. Jiang, M. Tinoco, A.B. Hungria, J. Han, G. Blanco, J.J. Calvino, X. Chen, Enhanced hydroxyl radical scavenging activity by doping lanthanum in ceria nanocubes, J. Phys. Chem. C 120 (2016) 1891–1901.
[25] X. Niu, M. Li, B. Hao, H. Li, Hydrothermal synthesis of 3D hierarchical porous CeO_2 rugby-ball-like nanostructures with nanorods as building blocks, J. Mater. Sci.: Mater. Electron. 27 (2016) 6845–6848.
[26] B. Jia, M. Qin, S. Li, Z. Zhang, H. Lu, P. Chen, H. Wu, X. Lu, L. Zhang, X. Qu, The synthesis of mesoporous single crystal $Co(OH)_2$ nanoplate and its topotactic conversion to dual-pore mesoporous single crystal Co_3O_4, ACS Appl. Mater. Interfaces 8 (2016) 15582–15590.
[27] J.Y. Luo, M. Ming, L. Xiang, X.G. Li, Y.Q. Zha, T.D. Hu, Y.N. Xie, Z. Jing, Mesoporous Co_3O_4–CeO_2 and Pd/Co_3O_4–CeO_2 catalysts: synthesis, characterization and mechanistic study of their catalytic properties for low-temperature CO oxidation, J. Catal. 254 (2008) 310–324.
[28] D.M.G. José, M. Gatica, Juan C. Hernández-Garrido, José J. Calvino, Gustavo A. Cifredo, Hilario Vidal, Experimental evidences of the relationship between reducibility and micro- and nanostructure in commercial high surface area ceria, Appl. Catal. A: General 479 (2014) 35–44.
[29] R. Shang, Y. Duan, X. Zhong, W. Xie, Y. Luo, L. Huang, Formic acid modified Co_3O_4-CeO_2 catalysts for CO oxidation, Catalysts 6 (2016) 48.
[30] A. Gupta, U. Waghmare, M. Hegde, Correlation of oxygen storage capacity and structural distortion in transition-metal-, noble-metal-, and rare-earth-ion-substituted CeO_2 from first principles calculation, Chem. Mater. 22 (2010) 5184–5198.
[31] L.-L. Huang, Y. Mao, G. Wang, X. Xia, J. Xie, S. Zhang, G. Du, G. Cao, X. Zhao, Ru-decorated knitted Co_3O_4 nanowires as robust carbon/binder-free catalytic cathode for lithium-oxygen batteries, New J. Chem. 40 (2016) 6812–6818.
[32] G. Pantaleo, V. La Parola, F. Deganello, R. Singha, R. Bal, A. Venezia, Ni/CeO_2 catalysts for methane partial oxidation: synthesis driven structural and catalytic effects, Appl. Catal. B 189 (2016) 233–241.
[33] X. Liu, K. Zhou, L. Wang, B. Wang, Y. Li, Oxygen vacancy clusters promoting reducibility and activity of ceria nanorods, J. Am. Chem. Soc. 131 (2009) 3140–3141.

[34] X. Liang, P. Liu, H. He, G. Wei, T. Chen, W. Tan, F. Tan, J. Zhu, R. Zhu, The variation of cationic microstructure in Mn-doped spinel ferrite during calcination and its effect on formaldehyde catalytic oxidation, J. Hazard. Mater. 306 (2016) 305–312.
[35] M.-T. Chen, C.-F. Lien, L.-F. Liao, J.-L. Lin, In-situ FTIR study of adsorption and photoreactions of CH_2Cl_2 on powdered TiO_2, J. Phys. Chem. B 107 (2003) 3837–3843.
[36] I.A. Fisher, A.T. Bell, In-Situ infrared study of methanol synthesis from H_2/CO_2 over Cu/SiO_2 and $Cu/ZrO_2/SiO_2$, J. Catal. 172 (1997) 222–237.
[37] R. Yang, Y. Fu, Y. Zhang, N. Tsubaki, In situ DRIFT study of low-temperature methanol synthesis mechanism on Cu/ZnO catalysts from CO_2-containing syngas using ethanol promoter, J. Catal. 228 (2004) 23–35.
[38] C.-C. Chuang, W.-C. Wu, M.-C. Huang, I.-C. Huang, J.-L. Lin, FTIR study of adsorption and reactions of methyl formate on powdered TiO_2, J. Catal. 185 (1999) 423–434.
[39] W.-C. Wu, C.-C. Chuang, J.-L. Lin, Bonding geometry and reactivity of methoxy and ethoxy groups adsorbed on powdered TiO_2, J. Phys. Chem. B 104 (2000) 8719–8724.